

Vibration control of high-rise buildings for wind: a robust passive and active tuned mass damper

Aly Mousaad Aly*

Department of Civil and Environmental Engineering, Louisiana State University, 3513D Patrick F. Taylor Hall, Baton Rouge, LA 70803, USA

(Received July 3, 2012, Revised May 25, 2013, Accepted July 5, 2013)

Abstract. Tuned mass dampers (TMDs) have been installed in many high-rise buildings, to improve their resiliency under dynamic loads. However, high-rise buildings may experience natural frequency changes under ambient temperature fluctuations, extreme wind loads and relative humidity variations. This makes the design of a TMD challenging and may lead to a detuned scenario, which can reduce significantly the performance. To alleviate this problem, the current paper presents a proposed approach for the design of a robust and efficient TMD. The approach accounts for the uncertain natural frequency, the optimization objective and the input excitation. The study shows that robust design parameters can be different from the optimal parameters. Nevertheless, predetermined optimal parameters are useful to attain design robustness. A case study of a high-rise building is executed. The TMD designed with the proposed approach showed its robustness and effectiveness in reducing the responses of high-rise buildings under multidirectional wind. The case study represents an engineered design that is instructive. The results show that shear buildings may be controlled with less effort than cantilever buildings. Structural control performance in high-rise buildings may depend on the shape of the building, hence the flow patterns, as well as the wind direction angle. To further increase the performance of the robust TMD in one lateral direction, active control using LQG and fuzzy logic controllers was carried out. The performance of the controllers is remarkable in enhancing the response reduction. In addition, the fuzzy logic controller may be more robust than the LQG controller.

Keywords: high-rise buildings; wind-induced vibration; robust control; tuned mass damper; optimal design; white-noise; LQG controller; fuzzy logic controller

1. Introduction

1.1 Background

In the past few decades, tuned mass dampers (TMDs) have been enjoying renewed interest as an attractive means for controlling infrastructure systems against severe wind and earthquake loading. TMDs have been implemented in structures to reduce wind-induced vibrations. For examples, TMDs have been installed in the following buildings/towers: the Citicorp Center Office Building in New York City, the Chiba Port Tower in Japan, the Centrepont Tower in Sydney, the John Hancock Tower in Boston, the Taipei 101 Tower in Taiwan and the Milad Tower in Iran

*Corresponding author, Assistant Professor, E-mail: aly@LSU.edu

(Ghorbani-Tanha *et al.* 2009). A TMD consists of a small spring-mass damped system connected to a primary structure (Fig. 1(a)). The frequency of the TMD is tuned to a particular structural frequency so when that frequency is excited the TMD will resonate and hence dissipate the input energy acting on the structure. Maximum response reduction in the primary structure is attained when the damping and tuning frequency ratios of the TMD system arrive at their optimal values. In any case, the tuning frequency of the TMD depends on the uncertain estimate of the natural frequency of the primary structure.

Although there have been advancements in finite element (FE) techniques and the fact that the frequency of the primary structure can be measured on-site during the installation of the TMD, uncertainties in the dominant frequency may exist. This may lead to a detuned scenario, where the performance of the device is dramatically reduced. The uncertainties can be a result of some localized damage or changes in the ambient conditions, such as, wind speed (aeroelastic effects, Gu and Peng 2002), temperature, relative humidity, building occupancy and other factors that might occur with the building during its service life. Even without evidence of structural damage, long-term monitoring studies reveal that structural modal frequencies exhibited substantial seasonal variation (Xia *et al.* 2006, Sohn *et al.* 1999, Lee and Yun 2006, Yuen and Kuok 2010). Clinton *et al.* (2006) analyzed long-term structural monitoring records of two reinforced concrete buildings. Under no structural damage, the background weather conditions, including rainfall and temperature variation, induced considerable fluctuation of the modal frequencies. According to Liu and DeWolf (2007), the maximum difference in the modal frequencies could be up to 6% under an overall temperature variation of 21°C.

A common technique that can help improve the robustness of the TMD under frequency changes is the use of an active tuned mass damper (ATMD). ATMDs are also known as hybrid mass dampers. An ATMD can be created by introducing an active control force to act between the primary structure and the TMD. By doing so, both the effectiveness and the robustness of the TMD can be enhanced. Investigations on the performance and design techniques of ATMDs have been carried out by many researchers (Gu and Peng 2002, Aly *et al.* 2008, Li *et al.* 2010, Lu *et al.* 2012, Aly 2012). Gu and Peng (2002) presented an experimental study of active control of wind-induced vibration of a tall building. Bani-Hani (2007) used neural networks for vibration control of wind-induced response of a tall building with an ATMD. Li *et al.* (2010) presented an optimum design methodology of an active tuned mass damper for asymmetric structures. Recently, Lu *et al.* (2012) conducted vibration control using ATMD and site measurements on the Shanghai World Financial Center Tower.

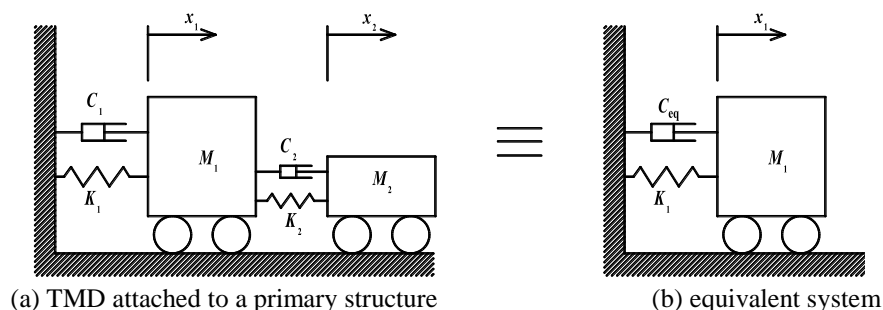


Fig. 1 (a) Primary structure (K_1 , M_1 and C_1) with tuned mass damper (K_2 , M_2 and C_2) and (b) the equivalent system

1.2 Paper layout

In this paper, a robust design of the TMD that accounts for structural uncertainties is developed for high-rise buildings under multidirectional wind loads. First, a numerical approach is proposed to evaluate the optimum parameters of the TMD for a primary structure. Generic design charts are created based on desired optimization objectives (displacement and acceleration), under different input excitations. Second, the optimum parameters are used to estimate the robust parameters for a structure with stiffness uncertainties. Finally, the TMD was attached to the top of a high-rise building exposed to multidirectional wind loads and its performance was studied. In addition, active control of the TMD with LQG and fuzzy logic controllers is executed to further enhance the performance. The paper is organized as follows. In section 2, the proposed optimization approach is presented. Section 3 describes a case study as an application example of a high-rise building. Section 4 utilizes the proposed methodology for the design of a robust passive and active TMD for the application example described in section 3. In section 5, the results are presented and discussed with comprehensive comments. Section 6 summarizes the conclusions drawn by the current study.

2. Optimization approach

2.1 Literature

According to Warburton and Ayorinde (1980), when determining optimum parameters for a TMD, the primary structure may be treated as an equivalent single degree-of-freedom system (SDOF) if its natural frequencies are well separated. The effect of the TMD can be viewed as being equivalent to changing the damping ratio of the original system from a value $\zeta_1 = C_1/2(K_1M_1)^{0.5}$ to a larger value ζ_e (Simiu and Scanlan 1996). The equivalent system has the same mass and stiffness as the primary structure but with damping $C_e = 2 \zeta_e (K_1M_1)^{0.5}$ as shown in Fig. 1(b). Using expressions from Simiu and Scanlan (1996) it can be shown that

$$\zeta_e = \frac{1}{2} \frac{\alpha_1(\alpha_2\alpha_3 - \alpha_1) - \alpha_0\alpha_3^2}{\alpha_0(\alpha_2\alpha_3 - \alpha_1) + \alpha_3(\beta_1^2 - 2\alpha_0) + \alpha_1} \tag{1}$$

in which

$$\left. \begin{aligned} \alpha_0 &= f^2; & \alpha_1 &= 2f(\zeta_1f + \zeta_2); & \alpha_2 &= 1 + f^2(1 + \mu) + 4f\zeta_1\zeta_2 \\ \alpha_3 &= 2\zeta_1 + 2\zeta_2f(1 + \mu); & \beta_1 &= 2\zeta_2f \end{aligned} \right\} \tag{2}$$

where

$$\mu = M_2 / M_1; \quad f = \omega_2 / \omega_1; \quad \omega_i = \sqrt{K_i / M_i}; \quad \zeta_i = C_i / (2M_i\omega_i). \tag{3}$$

For a certain tuning frequency ratio, f , the optimal value of the damping coefficient of the TMD that will minimize the displacement response of the primary structure under white-noise excitation is given by

$$\zeta_2^{opt} = \frac{\sqrt{\mu}}{2} \quad (4)$$

and the corresponding equivalent damping is

$$\zeta_e^{opt} = \frac{\sqrt{\mu}}{4} + 0.8\zeta_1 > \zeta_1. \quad (5)$$

Feng and Mita (1995) proposed formulae for estimating the optimum parameters of the TMD by minimizing the mean square response of the primary structure to a white-noise force excitation for wind analysis. For wind loading, they give the following absorber parameters

$$f = \frac{\sqrt{1+(\mu/2)}}{(1+\mu)}; \quad \zeta_2^{opt} = \frac{1}{2} \sqrt{(1+\mu)f^4 - \left(\frac{2+\mu}{1+\mu}\right)f^2 + \frac{1}{1-\mu}} \quad (6)$$

Numerical optimization under white-noise excitation

For wind-induced vibration of large-scale structures, vibration frequencies and damping modes may vary with wind speed. Because of this, the optimization is based on an input white-noise excitation. From Eq. (3), the mass, stiffness, and damping of the TMD can be written as functions of the mass ratio μ , the frequency ratio f , the TMD damping factor ζ_2 and the parameters of the primary structure as follows

$$M_2 = \mu M_1; \quad K_2 = \mu M_1 \omega_1^2 f^2; \quad C_2 = 2\mu M_1 \omega_1 f \zeta_2. \quad (7)$$

Equations of motion of the system shown in Fig. 1(a), when exposed to white-noise excitation, $w(t)$, can be written as

$$\mathbf{M}_s \ddot{\mathbf{q}}(t) + \mathbf{C}_s \dot{\mathbf{q}}(t) + \mathbf{K}_s \mathbf{q}(t) = \mathbf{G}w(t) \quad (8)$$

where the mass (\mathbf{M}_s), stiffness (\mathbf{K}_s) and damping (\mathbf{C}_s) matrices are characteristic of the structure and given by

$$\mathbf{M}_s = \begin{bmatrix} M_1 & 0 \\ 0 & M_2 \end{bmatrix}, \quad \mathbf{K}_s = \begin{bmatrix} K_1 + K_2 & -K_2 \\ -K_2 & K_2 \end{bmatrix}, \quad \mathbf{C}_s = \begin{bmatrix} C_1 + C_2 & -C_2 \\ -C_2 & C_2 \end{bmatrix}. \quad (9)$$

Utilizing Eq. (7), the above matrices can be written as

$$\mathbf{M}_s = M_1 \begin{bmatrix} 1 & 0 \\ 0 & \mu \end{bmatrix}; \quad \mathbf{K}_s = M_1 \omega_1^2 \begin{bmatrix} 1 + \mu f^2 & -\mu f^2 \\ -\mu f^2 & \mu f^2 \end{bmatrix}; \quad \mathbf{C}_s = M_1 \omega_1 \begin{bmatrix} 2\zeta_1 + 2\mu f \zeta_2 & -2\mu f \zeta_2 \\ -2\mu f \zeta_2 & 2\mu f \zeta_2 \end{bmatrix}. \quad (10)$$

In Eq. (8) $\mathbf{q}(t)$ is a vector of displacements, $w(t)$ is the external excitation (e.g., seismic or wind excitation), \mathbf{G} is the corresponding loading matrix, and the operator $[\cdot]$ indicates a derivative with respect to time. The system can be transformed into a first-order time invariant linear system (Aly and Christenson 2008)

$$\dot{\mathbf{z}}(t) = \mathbf{A}\mathbf{z}(t) + \mathbf{B}w(t); \quad \mathbf{Y}(t) = \mathbf{C}\mathbf{z}(t) + \mathbf{D}w(t) \quad (11)$$

where $\mathbf{z}(t)$ are the states of the system, $[\mathbf{A}, \mathbf{B}, \mathbf{C}, \text{ and } \mathbf{D}]$ are the associated state-space matrices,

and $\mathbf{Y}(t)$ is a vector of desired outputs, which is selected to include displacements and accelerations of the primary system and the inertial mass of the TMD.

Assuming that the external excitation $w(t)$ is a stationary white-noise, therefore, the states as well as the output of the linear system in Eq. (11) are stationary Gaussian processes. Making use of the stationary states, the time derivative of the covariance matrix of the states is set equal to zero

$$\frac{d}{dt}(E[\mathbf{z}\mathbf{z}^T]) = E[\dot{\mathbf{z}}\mathbf{z}^T + \mathbf{z}\dot{\mathbf{z}}^T] = 0 \quad (12)$$

Substituting Eq. (12) into the first part of Eq. (11) it can be shown that

$$\mathbf{A}E[\mathbf{z}\mathbf{z}^T] + E[\mathbf{z}\mathbf{z}^T]\mathbf{A}^T + \mathbf{B}E[ww^T]\mathbf{B}^T = 0. \quad (13)$$

The disturbance $w(t)$ on the system is a stationary white-noise such that $E[ww^T] = 2\pi S_0$ (Bendat and Piersol 2000). The Eq. (13) can then be rewritten as

$$\mathbf{A}E[\mathbf{z}\mathbf{z}^T] + E[\mathbf{z}\mathbf{z}^T]\mathbf{A}^T = -2\pi S_0 \mathbf{B}\mathbf{B}^T \quad (14)$$

where the covariance matrix of the states, \mathbf{z} , can be determined from Eq. (14) as the solution of the continuous time Lyapunov equation, for example, in MATLAB using the command *lyap.m* (Aly and Christenson 2008, Attaway 2009). The covariance matrix of the output, \mathbf{Y} , is determined from the covariance matrix of the states by employing the second part of Eq. (11), such as,

$$E[\mathbf{Y}\mathbf{Y}^T] = E[(\mathbf{C}\mathbf{z})(\mathbf{C}\mathbf{z})^T] + E[(\mathbf{D}w)(\mathbf{D}w)^T] = \mathbf{C}E[\mathbf{z}\mathbf{z}^T]\mathbf{C}^T + \mathbf{D}E[ww^T]\mathbf{D}^T. \quad (15)$$

Note that the output vector, \mathbf{Y} , gives the responses of the system as root mean square (RMS) values.

Relevant numerical techniques, which have been done with the help of MATLAB routines, are applied to solve the arising optimization problem and to find the optimum parameters of the TMD. For a given mass ratio, μ , one can assume a range of values for the frequency ratio, f , with a range of the damping factor, ζ_2 , to estimate the optimum parameters that minimize a certain desired output. Fig. 2 is an example of the numerical optimization carried out to estimate the optimal frequency ratio and damping factor of the TMD for two different mass ratios under wind loads modeled as white-noise. The optimization is based on the minimization of the displacement of the primary structure. In this numerical optimization, the responses of the primary structure are normalized, which means that the response obtained with the TMD attached to the structure is divided by the corresponding response obtained without the TMD. The optimal values of the frequency ratio and the damping factor of the TMD are written on the subfigures. It is shown that a TMD with 1% mass ratio can provide significant reduction in the displacement response of the primary structure. The reduction strongly depends on the tuning frequency and the damping ratio of the TMD. By increasing the mass ratio from 1% to 5%, the displacement response of the primary structure is further reduced. However, a TMD with 5% mass ratio is more robust to changes in the frequency ratio and the damping factor (the area indicating low normalized response in Fig. 2 (b) is larger than that of Fig. 2(a)).

Fig. 3 shows the normalized acceleration response of the primary structure for two different mass ratios (1% and 5%) under wind loads modeled as white-noise. It is shown that, by increasing the mass ratio, the reduction in the acceleration of the primary structure is increased. The optimal values of the damping factor for the two cases are similar to those obtained from the minimization

of the normalized displacement. However, the optimal value of the frequency ratio, which is different from that obtained by displacement minimization, is closer to 1. Like the displacement minimization objective, the TMD with 5% mass ratio is more robust to changes in the frequency ratio and the damping factor. This can be helpful when uncertainties in the frequency of the primary structure exist.

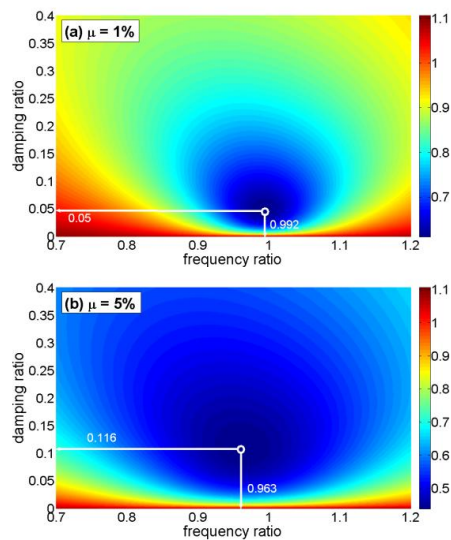


Fig. 2 Effect of changing the frequency and the damping ratios of the TMD on the normalized displacement of the primary structure: (a) 1% mass ratio and (b) 5% mass ratio

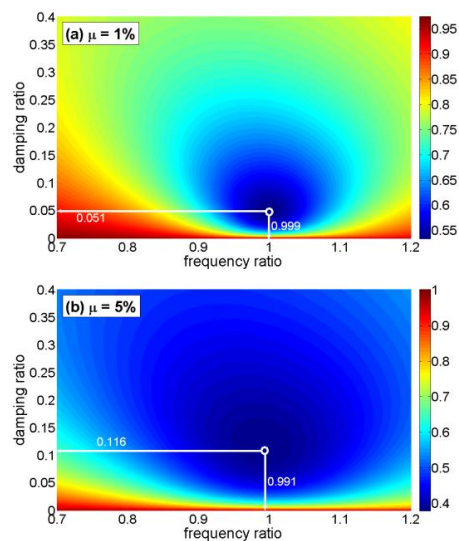


Fig. 3 Effect of changing the frequency and the damping ratios of the TMD on the normalized acceleration of the primary structure: (a) 1% mass ratio and (b) 5% mass ratio

One can create a design chart that is helpful in the design process of the TMD, by running the optimization simulations for different mass ratios and obtaining the corresponding optimal tuning frequencies and damping ratios of the TMD, based on minimization of displacement or acceleration. Fig. 4 presents the results when the optimization was carried out based on minimization of displacement and acceleration under wind and earthquake input excitations. The main difference between the wind and the earthquake input excitations is that the latter causes inertial loads on both the primary structure and the TMD (base excitation) while the wind load is considered external white-noise acting on the primary structure (force excitation).

For a certain primary structure under earthquake or wind excitation, one can obtain the uncontrolled displacement and acceleration response (without the TMD), then from Fig. 4 according to the required reduction in the displacement and/or the acceleration response, the required mass ratio of the TMD can be estimated. From Fig. 5, one can obtain the optimal tuning frequency and the damping ratio of the TMD. Fig. 4 provides the normalized displacement and acceleration response of the TMD as a function of the mass ratio. It is shown that the increase in the mass ratio reduces the response of the TMD.

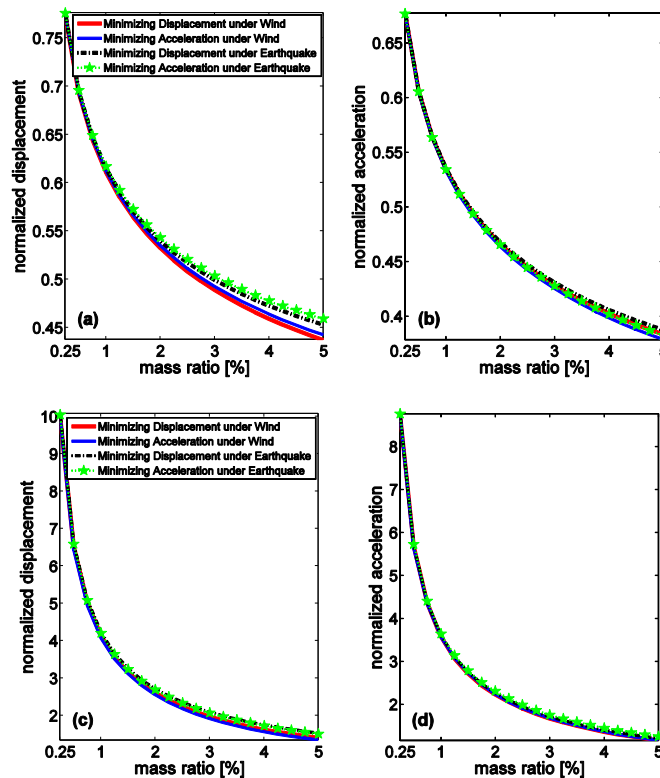


Fig. 4 Building and TMD normalized displacement and acceleration as a function of the TMD’s mass ratio: (a) building displacement, (b) building acceleration, (c) TMD displacement and (d) TMD acceleration

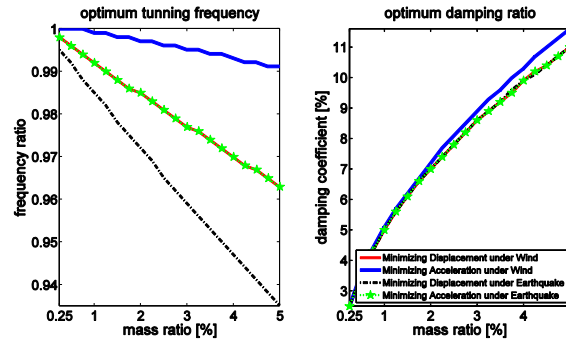


Fig. 5 Optimal frequency ratio and damping coefficient of the TMD as functions of the mass ratio

Table 1 Comparison between the optimal TMD design parameters obtained from the proposed technique and the literature

Mass ratio	Optimum Parameters	Simiu and Scanlan (1996)	Feng and Mita (1995)	Numerical optimization	
				Min. Disp.	Min. Accel.
1%	f_2/f_1	0.992	0.993	0.992	0.999
	ξ_e^{opt}	0.033	-	0.029	0.028
	ξ_2^{opt}	0.050	0.086	0.050	0.051
2%	f_2/f_1	0.985	0.985	0.985	0.997
	ξ_e^{opt}	0.043	-	0.038	0.036
	ξ_2^{opt}	0.071	0.122	0.070	0.072
3%	f_2/f_1	0.977	0.978	0.977	0.995
	ξ_e^{opt}	0.051	-	0.046	0.043
	ξ_2^{opt}	0.087	0.148	0.086	0.089
4%	f_2/f_1	0.970	0.971	0.970	0.993
	ξ_e^{opt}	0.058	-	0.052	0.048
	ξ_2^{opt}	0.100	0.171	0.099	0.103
5%	f_2/f_1	0.963	0.964	0.963	0.991
	ξ_e^{opt}	0.064	-	0.057	0.052
	ξ_2^{opt}	0.112	0.190	0.116	0.116

Table 1 lists the optimal parameters obtained by the proposed numerical approach along with optimal parameters taken from the literature (see section 2.1). It is shown that there is an excellent agreement between the proposed approach and the method provided in Simiu and Scanlan (1996) in predicting the optimal frequency and damping ratios when the objective is to minimize displacement. However, the equivalent structural damping obtained by the formula presented in Simiu and Scanlan (1996) is higher. Similarly, there is an excellent agreement between the values of the tuning frequency ratio and the values predicted by Feng and Mita (1995). But, the optimal damping ratio obtained from Feng and Mita is higher than the damping ratios obtained from the proposed approach and the formula given in Simiu and Scanlan (1996). Furthermore, the proposed approach can provide the optimum parameters when the objective is to minimize the acceleration response of the building.

3. An application example

To show the applicability of the proposed approach for the design of a robust tuned mass damper, a case study of a high-rise building exposed to multidirectional wind loads is carried out. This section of the paper gives a description of the building and a summary of the excitation wind loads.

3.1 Building's model

A numerical model representative of a full-scale concrete high-rise building excited by multidirectional wind loads is used as a case study. The building has a height of 221.3 m aboveground and a rectangular cross-section of $B/D = 2.56$ (B : chord length, D : thickness). The aspect ratio is nearly 10, which makes it very slender and sensitive to strong winds. The overall building's mass is about 1.4×10^5 tons. The structure has 50 stories aboveground level. There are four underground stories. The first six modes of vibration are shown in Fig. 6(a). The first six natural frequencies are: 0.122 Hz, 0.135 Hz, 0.461 Hz, 0.647 Hz, 1.079 Hz and 1.083 Hz, respectively. This building behaves in shear in the x-direction and as a cantilever in the y-direction (very slender); a detailed description of the building is provided in Aly (2009), Aly *et al.* (2011a) and Aly *et al.* (2012).

Although FE software packages can help to generate mode shapes, modal masses and modal frequencies for a desired number of modes, this software does not provide information about damping in buildings. This is because, unlike mass and rigidities that are distributed along the structural elements, damping is related to friction in joints and hysteresis in the material. There is no convenient means of refining the predictive capabilities regarding inherent structural damping. While the best way to obtain information about damping is the on-site measurements, there have been some efforts to develop empirical predictive tools for damping estimation based on full-scale observations (Li *et al.* 2002, Satake *et al.* 2003, Smith and Willford 2007). Tamura and Yoshida (2008) presented a damping predictor for high-rise buildings that is dependent on the amplitude of the displacement response. The formula for reinforced concrete buildings is given by

$$z = \frac{0.93}{H} + 470 \frac{x_H}{H} - 0.0018 \quad (16)$$

where ζ is the first modal damping, x_H is the displacement at the top of the building, and H is the building's height. For $x_H = 0.5$ m and overall building height of about 240 m (including underground stories), the damping factor from the above equation is about 1%. For $x_H = 0.25$ m and 1 m the corresponding damping factors are 5% and 2% respectively. However, the damping factor for this building is assumed to be 1%.

For control purposes, a lumped masses model is derived from the original FE model. In this model, the mass of the building is lumped at the positions of floors (Fig. 6(b)). In general, the equation of motion for an n -story building moving in both the two transverse directions and in torsion may be written as

$$\mathbf{M}_s \ddot{\mathbf{x}} + \mathbf{C}_s \dot{\mathbf{x}} + \mathbf{K}_s \mathbf{x} = -\mathbf{F} + \Lambda \mathbf{f} \quad (17)$$

where $\mathbf{x} = [\mathbf{X} \ \mathbf{Y} \ \Theta]^T$. The terms $\mathbf{X} = [x_1 \ x_2 \ \dots \ x_n]$ and $\mathbf{Y} = [y_1 \ y_2 \ \dots \ y_n]$ are row vectors of the displacements of the center of mass of each floor in the x and y directions respectively, and $\Theta = [\theta_1 \ \theta_2 \ \dots \ \theta_n]$ is a vector of rotations of each floor about the vertical axis (z -axis) while n is the number of floors. \mathbf{M}_s , \mathbf{K}_s , and \mathbf{C}_s are mass, stiffness, and damping matrices, respectively. The mass matrix \mathbf{M}_s has the following form

$$\begin{bmatrix} \mathbf{M} & \mathbf{0} & \mathbf{0} \\ \mathbf{M}_s & \mathbf{0} & \mathbf{0} \\ \mathbf{0} & \mathbf{0} & \mathbf{I} \end{bmatrix} \quad (18)$$

where $\mathbf{M} = \text{diag}([m_1 \ m_2 \ \dots \ m_n])$ is a diagonal $n \times n$ matrix of masses of each floor, and $\mathbf{I} = \text{diag}([I_1 \ I_2 \ \dots \ I_n])$ where I_i is the moment of inertia of the i^{th} floor. The stiffness matrix \mathbf{K}_s is obtained by assuming the stiffness between adjacent floors as a combination of cantilever and shear rigidities. MATLAB codes were written to derive the best stiffness matrix that provides the closest mode shapes to those of the FE model and almost same first six natural frequencies. The stiffness matrix \mathbf{K}_s has the form

$$\begin{bmatrix} \mathbf{K}_x & \mathbf{0} & \mathbf{0} \\ \mathbf{K}_s & \mathbf{0} & \mathbf{0} \\ \mathbf{0} & \mathbf{0} & \mathbf{K}_\theta \end{bmatrix} \quad (19)$$

where \mathbf{K}_x , \mathbf{K}_y and \mathbf{K}_θ are the stiffness matrices in the transverse directions (x and y) and about the z -axis (torsion), respectively. An uncertainty of $\pm 10\%$ in the structural stiffness matrix (corresponding to uncertainty in the natural frequency of about $\pm 5\%$) is assumed to investigate the robustness of the control system.

The most effective way to treat damping within a modal analysis framework is to consider the damping value as an equivalent Rayleigh Damping in the form of (Chowdhury and Dasgupta 2003)

$$\mathbf{C}_s = \alpha \mathbf{M}_s + \beta \mathbf{K}_s \quad (20)$$

in which \mathbf{C}_s is the damping matrix; α and β are pre-defined constants. After calculating the damping matrix, the modal damping vector was estimated for all the vibrational modes and the first six modal damping ratios were assigned to the value of 1%. The damping matrix is

reconstructed using the new modal damping vector as follows (Meirovitch 1967). At normal modes, when the equations of motion are decoupled, the equations of motion for free damped vibration take the form,

$$M_s \ddot{x} + C_D \dot{x} + K_s x = 0 \tag{21}$$

where

$$C_D = [uu]^T [C_s] [uu] = 2M_s [w][z] \tag{22}$$

in which $[uu]$ is a matrix of orthonormal modes associated with the eigenvalue problem (eigenvectors), $[w]$ is a diagonal matrix of undamped natural frequencies and $[z]$ is a diagonal matrix of modal damping.

In Eq. (17), the disturbance $\mathbf{F} = [\mathbf{F}_x \ \mathbf{F}_y \ \mathbf{T}]^T$ is a vector of excitation in which \mathbf{F}_x and \mathbf{F}_y are two vectors of horizontal loads acting in the x and y directions, respectively; \mathbf{T} is a vector of external torsional wind loads; \mathbf{f} is a vector of control forces and its coefficient matrix Λ is determined by location of control devices.

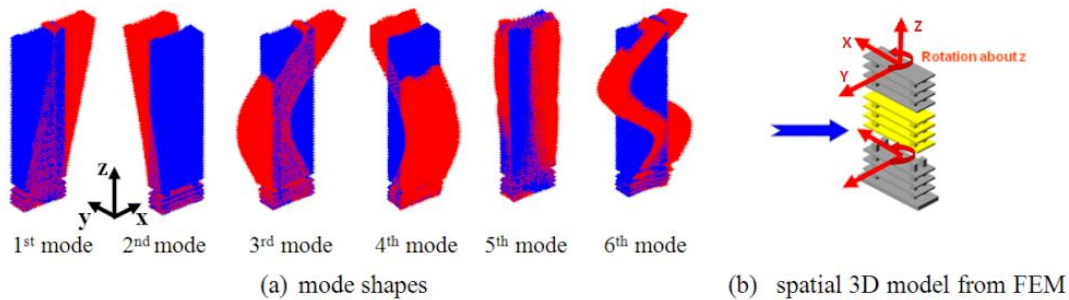


Fig. 6 FE model of the tower with the coordinate system: note that the wind direction 0° is along the x -axis

3.2 Wind loading

Wind loading vectors (\mathbf{F}_x , \mathbf{F}_y , and \mathbf{T}) lumped at the position of floors were obtained from wind tunnel pressure tests conducted on a scaled 1:100 rigid model of the building (Aly 2009). The wind profile represents a typical urban terrain exposure as shown in Fig. 7. The reference mean wind speed was measured at a height of 1 m. The prototype reference mean wind speed is dependent on the wind direction angle (Fig. 7). The target for the wind profiles is Eurocode 1 (2004). The surrounding buildings within a radius of 500 m from the center of the building were also scaled 1:100 and presented in the test section (Fig. 8). Pressure taps were distributed on the outer surface of the test model. To allow for sufficient pressure measurements, 400 taps were mapped on the outer surface of the model. Pressure data were collected at a frequency of 62.5 Hz. Further details about the wind tunnel experiment are provided in Aly (2009) and Rosa *et al.* (2012).

Pressure data were integrated on the outer surface of the building to obtain time histories of wind loads. For the estimation of the wind loads at each floor, the tributary area for each floor was divided into smaller areas and the time history of the wind loads at each area was evaluated by

using the C_p (pressure coefficient) records of the closest pressure tap (see Fig. 9). Codes were written in MATLAB to estimate the time histories of the wind forces acting at the center of each smaller area. After that, the floor forces in the two directions were obtained from the summation of the forces in each lateral direction. The torsion at each floor is the result of the summation of the force moments about the floor vertical axis.

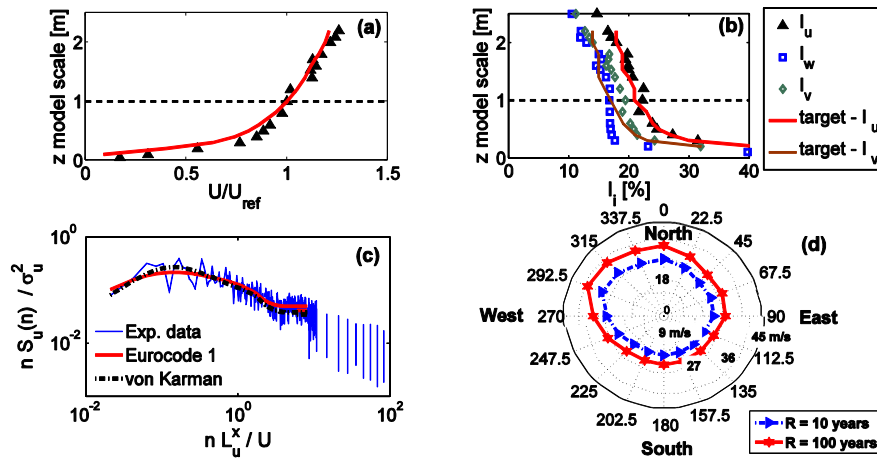


Fig. 7 (a) Mean wind speed profile, (b) turbulence intensity profiles, (c) wind spectra and (d) wind speed directionality. U is the mean wind speed (in the along wind direction), U_{ref} is the reference mean wind speed, I_i is the turbulence intensity, n represents the fluctuation frequency, S_u is the spectral density of the along wind velocity component, σ_u is the root mean square value of the velocity, and L_u^x is the integral length scale (more details are given in Aly (2009) and Rosa *et al.* (2012))



Fig. 8 A photograph of the wind tunnel test set up of the building and its surrounding (see Zasso *et al.* 2008 and Aly 2009)

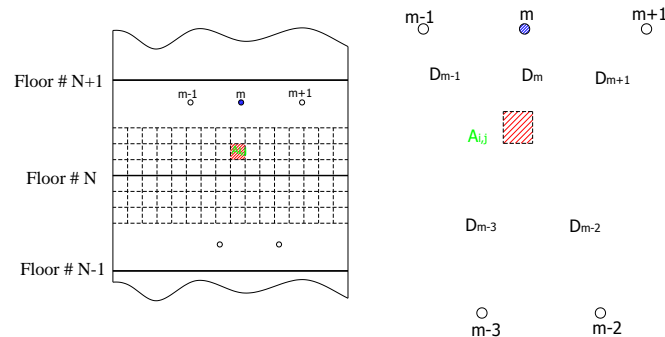


Fig. 9 Wind load estimation from pressure data: the tributary area of floor # N was divided into smaller areas; the pressure forces acting on each smaller area, $A_{i,j}$, were calculated based on the pressure data acquired at the nearest pressure tap, m

4. Passive and active tuned mass damper design

In this section, the proposed approach for the design of a robust TMD is followed using the case study building described in section 3. A passive robust TMD design is carried out. To further increase the performance, an active control force acting between the building and the TMD is created using two controllers.

4.1 Robust TMD design

Two TMD designs are proposed: first, the optimum parameters of the TMD for the nominal structure, that is the building with 0% stiffness uncertainty, are estimated; second, the parameters are obtained for the building with uncertainty in its stiffness ($\pm 10\%$). Fig. 10 shows the effect of the TMD mass ratio on the RMS and peak accelerations of the building with stiffness uncertainties (x-direction under wind direction of 292.5° , where the worst uncontrolled response was observed). It is shown that by increasing the mass ratio the accelerations are significantly reduced. A TMD with a mass ratio of 2% is capable of maintaining the acceleration perception lower than the maximum allowable comfort limit (20 milli-g).

Fig. 11 shows the influence of the TMD mass ratio on the RMS and peak accelerations of the building with stiffness uncertainties (y-direction under wind direction of 0° , where the worst uncontrolled response was observed). The figure shows that by increasing the mass ratio the accelerations are significantly reduced. However, a TMD with a mass ratio of 5% is not able to maintain the accelerations lower than the maximum allowable values. However, a mass ratio of 3% was considered in the y-direction and the design an ATMD was carried out.

4.2 ATMD design

The ATMD is actually a combination of the TMD and an active control actuator (see Fig. 12). The efficiency of the ATMD relies on the forces generated by the control actuator. A typical ATMD requires less energy to operate than a fully active mass damper system.

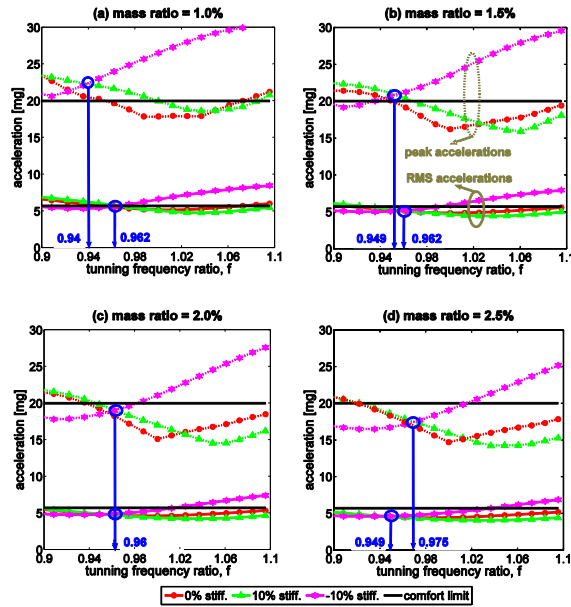


Fig. 10 Effect of the TMD mass ratio on the acceleration response of the building under wind (x-direction). Note: the blue circle with an arrow indicates the tuning frequency ratio, f , which gives the minimum response under stiffness uncertainty

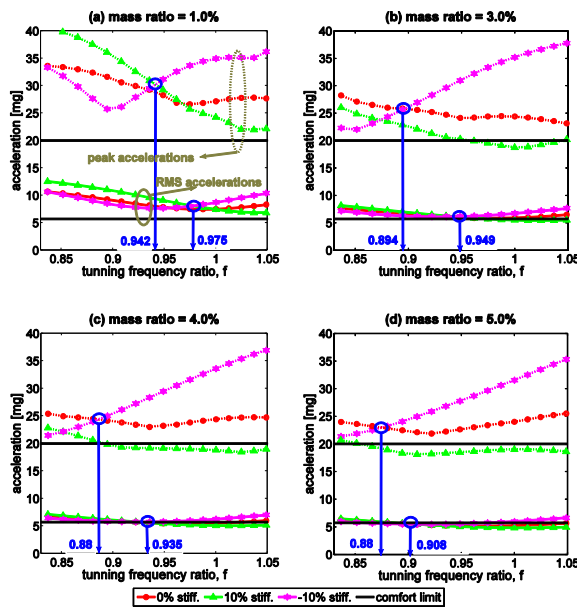


Fig. 11 Effect of the TMD mass ratio on the acceleration responses (y-direction). Note: the blue circle with an arrow indicates the tuning frequency ratio, f , which gives the minimum response under stiffness uncertainty

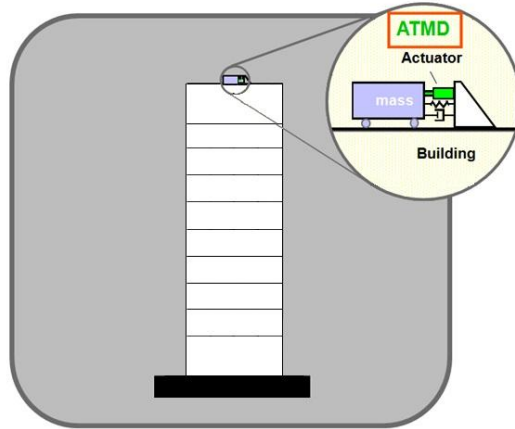


Fig. 12 Schematic of an active tuned mass damper (ATMD) installed on a high-rise building

Since the building’s mass is symmetrical, and the study is based on the assumption that the structure is responding in the linear region, the lateral and the torsional behavior of the building may be studied alone, then the response time histories can be combined simultaneously. In the current study, the plane motion of the structure in the x-direction is controlled using a TMD. However, since the control of the response in the x-direction will not affect the response of the building in the y-direction, an ATMD was designed to control the lateral in-plane response in the y-direction. Following that, the uncontrolled torsional response is added simultaneously to the two lateral responses to represent the overall response in the two lateral directions.

For a building equipped with ATMD and performing lateral in-plane motion (e.g., y-direction) under wind loads, the equation of motion can be written as

$$M\ddot{\mathbf{X}} + C_y\dot{\mathbf{X}} + K_y\mathbf{X} = -\mathbf{F}_y + \Lambda f_y \tag{23}$$

It is important to note that the size of structure, and therefore the number of degrees of freedom, is an important factor in the whole computation effort. It is essential to use reduced-order methods to make the computation practical for a real structure. Using observability and controllability of the structure, one can eliminate many degrees of freedom. The state reduction approach derived by Davison (1966) and summarized later in Wu *et al.* (1998) is used in the current paper (see also Lu *et al.* 2003). In this approach, the 55 degree-of-freedom (DOF) in-plane system is reduced to 15 DOF where the first 30 modes are retained. Note that the condition for this approach was that the response in terms of displacements and accelerations of the 15 DOF and 55 DOF are very much the same (see Aly *et al.* 2012). This model is referred to as Reduced Order System (ROS). The state equation of the ROS that corresponds to the full order system (FOS) in Eq. (23) is expressed as

$$\dot{\mathbf{z}} = \mathbf{A}\mathbf{z} + \mathbf{B}f + \mathbf{E}w_y \tag{24}$$

in which $\mathbf{z} = [\mathbf{X}, \dot{\mathbf{X}}]$ is a 32-dimensional state vector, \mathbf{X} is a vector of the in-plane displacements of floors -2, 2, 5, 9, 13, 17, 20, 25, 28, 32, 35, 39, 42, 45 and 50 in addition to the

displacement of the inertial mass of the damper; \mathbf{A} is a (32×32) system matrix; \mathbf{B} is a 32-dimensional location vector; and \mathbf{E} is a 32-dimensional excitation vector. For the ROS, the wind loads acting on each of the 15 floors were computed from the wind loads acting on each of the 55 floors by lumping wind forces on adjacent floors. The controlled output vector, \mathbf{y}_c , and the measured output, \mathbf{y}_m , of the ROS described by Eq. (24) is expressed as

$$\left. \begin{aligned} y_c &= \mathbf{C}_c \mathbf{z} + \mathbf{D}_c f + \mathbf{F}_c \mathbf{w}_x \\ y_m &= \mathbf{C}_m \mathbf{z} + \mathbf{D}_m f + \mathbf{F}_m \mathbf{w}_x + v \end{aligned} \right\} \quad (25)$$

where \mathbf{C}_c ; \mathbf{D}_c ; \mathbf{F}_c ; \mathbf{C}_m ; \mathbf{D}_m ; \mathbf{F}_m are matrices with appropriate dimensions and v is a measurement noise vector. The model used for controller design was further reduced as follows

$$\left. \begin{aligned} \dot{\mathbf{z}}_r &= \mathbf{A}_r \mathbf{z}_r + \mathbf{B}_r f + \mathbf{E}_r \mathbf{w}_x \\ y_{cr} &= \mathbf{C}_{cr} \mathbf{z}_r + \mathbf{D}_{cr} f + \mathbf{F}_{cr} \mathbf{w}_x \\ y_{mr} &= \mathbf{C}_{mr} \mathbf{z}_r + \mathbf{D}_{mr} f + \mathbf{F}_{mr} \mathbf{w}_x + v_r \end{aligned} \right\} \quad (26)$$

where \mathbf{z}_r is a 6-dimensional state vector of the reduced order system; \mathbf{y}_{cr} is a controlled output vector identical to \mathbf{y}_c , which is defined by Eq. (25); \mathbf{y}_{mr} is the measured output vector; v_r is the measurement noise vector and \mathbf{C}_{cr} ; \mathbf{D}_{cr} ; \mathbf{F}_{cr} ; \mathbf{C}_{mr} ; \mathbf{D}_{mr} and \mathbf{F}_{mr} are appropriate matrices.

In order to make the design of such a control system more realistic and applicable, the following assumption and constraints are applied:

- The parameters of the ATMD in terms of mass, stiffness, and damping are kept the same as those of the TMD;
- The maximum capacity of the actuator is constrained to 200 kN. It is worth noting that increasing the maximum allowable control force results in an increase in the actuator's stroke;
- The computational delay and the sampling rate of the digital controller is 1/1024 s. This is the same rate as some current available accelerometers;
- Three acceleration measurements are available at: floor 29, roof and the inertial mass of the ATMD.

4.2.1 LQG controller

A Linear-quadratic Gaussian regulator (LQG) design with output weighting is considered, to provide the desired control force using the MATLAB function (lqry.m). The state-feedback law $f = -\mathbf{Gz}_r$ minimizes the cost function

$$J(f) = \int_0^{\infty} (\mathbf{y}'_{mr} \mathbf{Q} \mathbf{y}_{mr} + f' \mathbf{R} f) dt \quad (27)$$

where \mathbf{G} is the feedback gain matrix, \mathbf{z}_r is a 6-dimensional state vector of the reduced order system, \mathbf{y}_{mr} is the measured output vector, the symbol (') denotes transpose, and \mathbf{Q} and \mathbf{R} are weighting matrices. Parametric studies were performed with various weighting matrices \mathbf{Q} , corresponding to various regulated output vectors. The results of these parametric studies indicated that an effective controller could be designed by selecting a vector of regulated responses to include velocities the floors.

Similar to the approach discussed in Dyke *et al.* (2003) and Yang *et al.* (2004), the optimal

control gain \mathbf{G} is obtained as (see also Skelton 1988)

$$\mathbf{G} = \bar{\mathbf{R}}^{-1}(\mathbf{B}'_r \mathbf{P}_c + \bar{\mathbf{S}}') \tag{28}$$

In which \mathbf{P}_c is the solution of the Riccati equation

$$\left. \begin{aligned} \mathbf{P}_c \bar{\mathbf{A}} + \bar{\mathbf{A}}' \mathbf{P}_c - \mathbf{P}_c \mathbf{B}_r \bar{\mathbf{R}}^{-1} \mathbf{B}'_r \mathbf{P}_c + \bar{\mathbf{Q}} - \bar{\mathbf{S}} \bar{\mathbf{R}}^{-1} \bar{\mathbf{S}}' &= 0 \\ \bar{\mathbf{Q}} &= \mathbf{C}'_{cr} \mathbf{Q} \mathbf{C}_{cr}; \bar{\mathbf{R}} = \mathbf{D}'_{cr} \mathbf{Q} \mathbf{D}_{cr} + \mathbf{R}; \bar{\mathbf{S}} = \mathbf{C}'_{cr} \mathbf{Q} \mathbf{D}_{cr}; \bar{\mathbf{A}} = \mathbf{A}_r - \mathbf{B}_r \bar{\mathbf{R}}^{-1} \bar{\mathbf{S}}' \end{aligned} \right\} \tag{29}$$

The reduced order state feedback, \mathbf{z}_r , is obtained using an observer based, on the separation principal. The Kalman-Bucy filter (e.g., Skelton 1988, Spencer *et al.* 1998) is used to estimate the observed states as explained in Yang *et al.* (2004).

4.2.2 Fuzzy logic controller

From a design point of view, fuzzy logic controllers do not require the complexity of a traditional control system. The measured accelerations can be used directly as inputs to the fuzzy logic controller. The main advantages of using a fuzzy logic control algorithm are summarized in Battaini *et al.* (1998) and Samali *et al.* (2004). According to Samali *et al.* (2004), uncertainties of input data are treated in a much easier way by fuzzy control theory than by classical control theory. Since fuzzy controllers are based on linguistic synthesis, they possess inherent robustness. Fuzzy controllers can be easily implemented in a fuzzy chip with immediate reaction time and autonomous power supply. Furthermore, the design of a fuzzy controller does not require a state reduction or any concern about observers. Only two acceleration measurements were used (floor 29 and the roof).

Fuzzy logic controllers are composed of the following steps (Aldawod *et al.* 2001, Marazzi and Magonette 2001):

- (1) Fuzzification: where the crisp value of the input is converted to a fuzzy linguistic value using membership functions.
- (2) Decision-making: which uses “IF-THEN” rules created based on expert control knowledge to correlate the linguistic variables of the input to linguistic variables of the output.
- (3) Defuzzification: where the fuzzy output is converted to a crisp control value.

The fuzzy logic system used in the current study is a Mamdani type, as presented in Fig. 13. The input variables to the fuzzy controller are selected to include accelerations of floor 29 and the roof while the output is the desired control force. The membership functions for the inputs are defined as seven triangles with overlaps, as indicated in Fig. 14. For the output, the membership function is defined as nine triangles with overlaps as shown in the same figure. The fuzzy variables used to define the fuzzy space are ZR (zero), PVS (positive very small), PS (positive small), PM (positive medium), PL (positive large), PVL (positive very large), NVS (negative very small), NS (negative small), NM (negative medium), NL (negative large) and NVL (negative very large). The rule-base for estimating the desired control force is presented in Table 2 (Samali *et al.* 2004).

For the same rule base, by adjusting the input and output membership functions and the limits of the input and the output variables, one can have families of controllers. Note the special adjustment of the three central membership functions (NVS, ZR, and PVS) of the output control force. This adjustment is done to reduce the output control forces at low system response, which improved the stability of the control system. A SIMULINK (Attaway 2009) model of the fuzzy logic controller implemented in the building-TMD system is shown in Fig. 15.

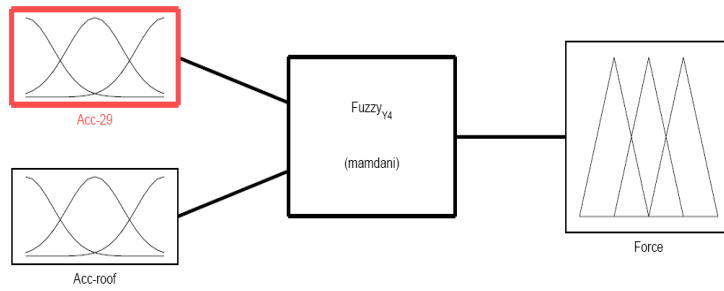


Fig. 13 Schematic of a fuzzy logic controller with two inputs and one output

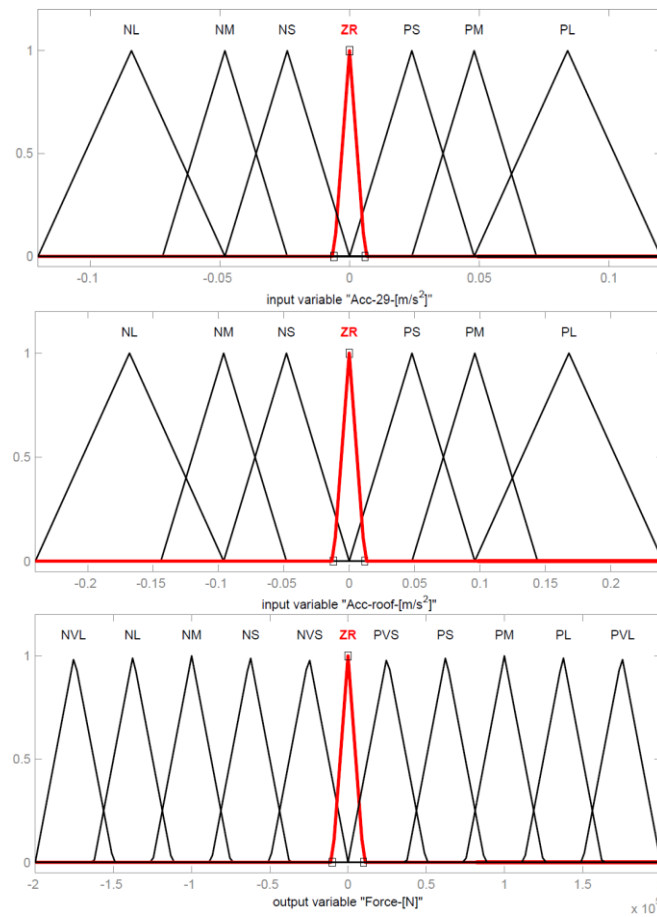


Fig. 14 Membership functions for the input accelerations and the output control force

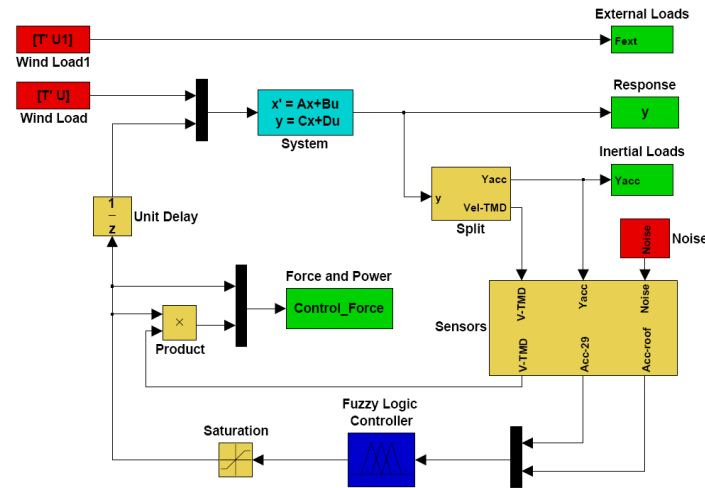


Fig. 15 Simulink model of the controlled structure with the fuzzy logic controller

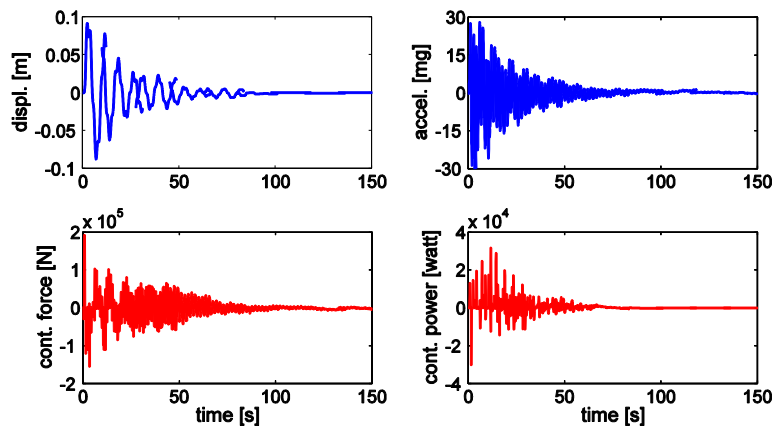


Fig. 16 Stability test of the fuzzy logic controller

Table 2 Fuzzy logic control rule base

Acceleration of the roof	Acceleration of 29 th floor						
	NL	NM	NS	ZR	PS	PM	PL
NL	PVL	PVL	PL	PVS	ZR	ZR	ZR
NM	PL	PL	PM	PVS	ZR	ZR	ZR
NS	ZR	NVS	PM	PS	PVS	ZR	ZR
ZR	ZR	ZR	NVS	ZR	PVS	ZR	ZR
PS	ZR	ZR	NVS	NS	NM	PVS	ZR
PM	ZR	ZR	ZR	NVS	NM	NL	NL
PL	ZR	ZR	ZR	NVS	NL	NVL	NVL

Although the fuzzy controller does not have a mathematical model to check its stability, some stability analysis criteria are proposed in the literature (Yan *et al.* 1994, Casciati 1997). One of the proposed methods to ensure stability is the phase plane trajectory, which is a technique to reflect graphically the dynamic properties of a control system in a phase plane. In this technique, the controller's stability can be checked through the ability of the controlled system to return to rest conditions following oscillations caused by an external disturbance. A stability test was performed considering the system with particular initial conditions on the state vector x and checking the ability of the controller to reach equilibrium after the transient phase. Fig. 16 shows the stability test of the fuzzy controller in terms of displacement response, acceleration response, control force, and control power. The figure shows the ability of the fuzzy controller to bring the system to rest after an initial excitation (decay), which demonstrates the system stability.

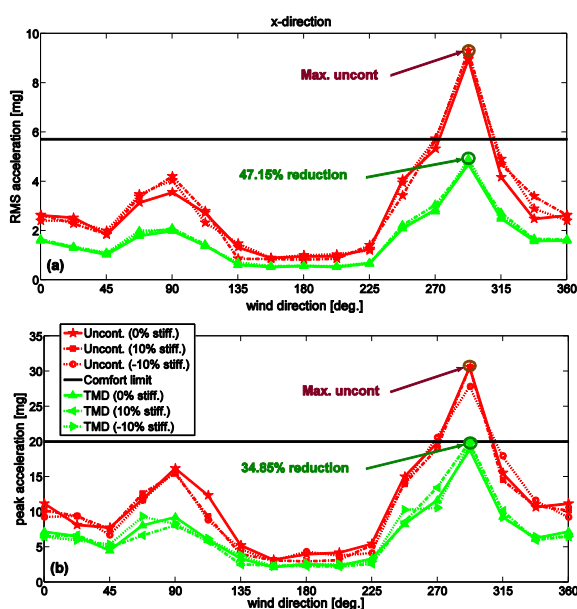


Fig. 17 Uncontrolled and controlled accelerations in the x-direction: (a) RMS values and (b) peak values

5. Results and discussion

5.1 X-direction

Fig. 17 shows controlled (with TMD) and uncontrolled acceleration responses of the building, in the x-direction under multidirectional wind loads. For comfort concerns, mean wind speed that corresponds to a return period of 10 years is considered. The controlled and uncontrolled responses of the building were evaluated by simulations. In the figures, “Uncont.” refers to the uncontrolled acceleration response of the building (without TMD) while “TMD” refers to the acceleration response of the building with TMD. RMS and peak accelerations were calculated for all the floors of the building, and the maximum value was taken. It was noticed during the calculations that the last floor has the maximum RMS and peak accelerations over all the building's floors. Uncertainty

in the stiffness of the building of $\pm 10\%$ is considered. In the figures, “0% stiff.” refers to the building with the original stiffness, “+10% stiff.” denotes the building with 10% increase in the original stiffness, and “-10% stiff.” designates the building with 10% reduction in the original stiffness.

The figure shows that, for wind loads with a return of 10 years, a TMD with a mass ratio of 2% (inertial mass of the TMD to the generalized mass of the building in the x-direction) can reduce the acceleration responses, in terms of RMS and peak values, lower than the maximum allowable values (RMS acceleration = 5.7 milli-g and peak acceleration = 20 milli-g). The TMD is capable of achieving response reduction over all the wind direction angles. The figure is superimposed by ellipses indicating the most unfavorable responses (uncontrolled and controlled by the TMD). The amount of reductions in the highest responses achieved by the TMD over the worst uncontrolled response is indicated in the figure. The capability of the TMD to significantly reduce the building response under uncertainty in the stiffness indicates that a robust design is achieved.

Table 3 lists the uncontrolled and controlled responses of the building in the x-direction under a wind attack angle of 292.5° . For security concerns, mean wind speed that corresponds to a return of 100 years is used. RMS and peak values of the displacement at the top corner of the building, RMS and peak values of maximum inter-story drift, RMS and peak values of shear loads (SL) at the ground level, and RMS and peak values of the bending moment (BM) at the ground level are considered. Percentages of response reductions are indicated in the table (between brackets). Under wind loads with a return of 100 years, the results show that the TMD can provide significant reductions in the displacement and the inter-story drift of the building. The design loads are reduced by about 20% to 46%.

Table 3 Uncontrolled and controlled (with TMD) building responses for security reasons (x-direction at 0° , R = 100 years)

Criteria	Uncontrolled			TMD		
	+0%	+10%	-10%	+0%	+10%	-10%
RMS Disp. (m)	0.2624	0.2636	0.2656	0.1439 (45.16%)	0.1397 (47.00%)	0.1693 (36.26%)
Peak Disp. (m)	0.8594	0.7909	0.7813	0.5356 (37.68%)	0.5164 (34.71%)	0.6073 (22.27%)
Peak Drift (rad)	0.0044	0.0041	0.0042	0.0028 (36.36%)	0.0028 (31.71%)	0.0032 (23.81%)
RMS BS (N)	8.63E+6	9.78E+6	8.16E+6	5.22E+6 (39.46%)	5.56E+6 (43.18%)	5.44E+6 (33.39%)
Peak BS (N)	29.57E+6	31.09E+6	26.57E+6	22.0E+6 (25.77%)	21.0E+6 (32.45%)	21.3E+6 (19.77%)
RMS BM (N.m)	12.72E+8	14.31E+8	11.80E+8	7.14E+8 (43.88%)	7.63E+8 (46.67%)	7.54E+8 (36.16%)
Peak BM (N.m)	43.67E+8	43.26E+8	35.14E+8	26.5E+8 (39.23%)	28.6E+8 (33.98%)	27.4E+8 (22.03%)

5.2 Y-direction

Fig. 18 shows controlled and uncontrolled acceleration responses of the building in the y-direction under wind loads with different direction angles. Two examples of control techniques are considered, TMD and ATMD (with LQG and fuzzy logic controllers). For each example, the

controlled response is plotted with the uncontrolled response. In the figure, “ATMD-LQG” refers to the acceleration response obtained when an ATMD with a LQG controller was implemented in the building, and “ATMD-Fuzzy” refers to the response with a fuzzy logic controller.

The figure shows that, under wind loads with a return of 10 years, a TMD with a mass ratio of 3% (inertial mass of the TMD to the generalized mass of the building in the y-direction) is not able to reduce the acceleration response in terms of RMS and peak values lower than the maximum allowable values for two wind direction angles (0° and 292.5°). The TMD is capable of achieving significant response reductions over all the other wind direction angles. Fig. 18 is superimposed by ellipses indicating the most unfavorable responses (uncontrolled, TMD, ATMD-LQG, and ATMD-Fuzzy). The amount of reductions in the highest responses achieved by the TMD and the ATMD over the worst uncontrolled response (for all the wind direction angles) is indicated in the figure. Again, like the case in the x-direction, uncertainty in the building’s stiffness indicates that the TMD is robustly designed (to reduce RMS accelerations).

Generally, the TMD gave significant reductions in the RMS and peak accelerations in both x and y-directions for all the wind direction angles. However, the TMD in the y-direction required heavier mass (the mass of the TMD in the x-direction is about two-thirds of the mass in the y-direction), and is shown to be unable to meet the comfort perception. This is because the acceleration responses (especially at the wind direction angle of 0°) in the y-direction are larger than those in the x-direction (at angle 292.5°). This may be attributed to the fact that the structure is more slender along the x-axis, which makes the flow reattachment occur more properly in the y-direction than in the x-direction (see Zasso *et al.* 2008). That is the flow patterns around the building under the wind direction angles of 0° and 292.5° are different, which arises a conclusion that structural control performance in high-rise buildings may depend on the shape of the building and the wind direction angle.

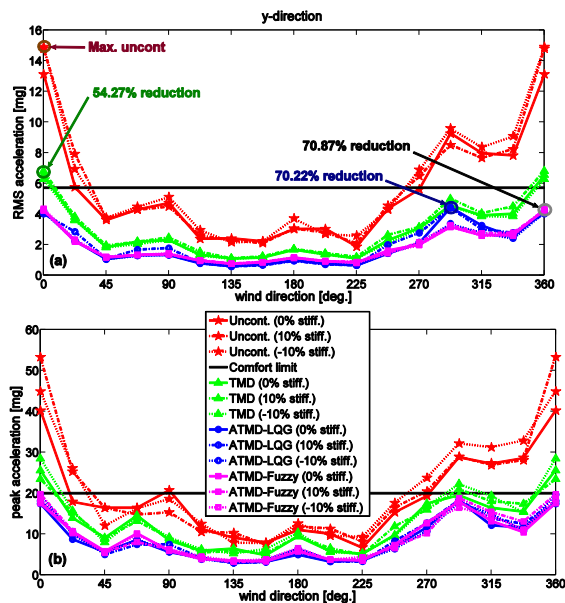


Fig. 18 Uncontrolled and controlled accelerations in the y-direction: (a) RMS values and (b) peak values

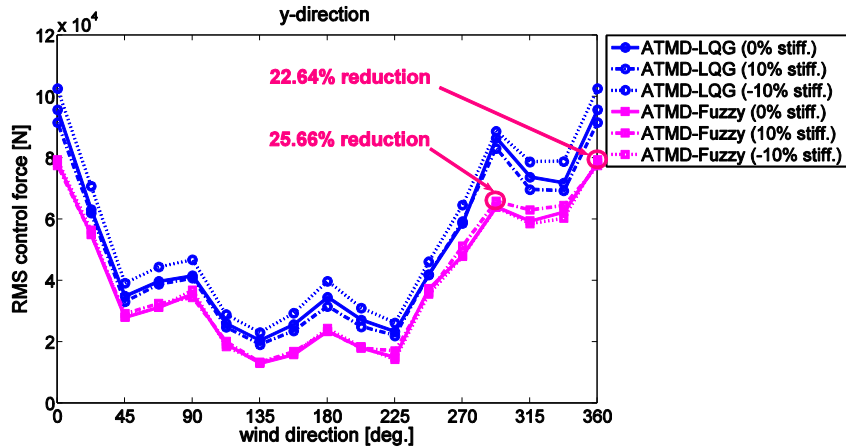


Fig. 19 RMS control forces of the LQG and the fuzzy logic controllers

ATMD-LQG and ATMD-fuzzy are capable of reducing the acceleration response in terms of RMS and peak values lower than the maximum allowable values. However, ATMD-fuzzy is shown to be more robust than ATMD-LQG (in reducing RMS accelerations). The robustness of the fuzzy logic controllers was also documented in Samali *et al.* (2004) and Aly *et al.* (2011a).

Fig. 19 shows the RMS values of the control forces generated by the LQG and the fuzzy logic controllers over all the wind direction angles. Not only the fuzzy logic controller is robust, but also it requires lower control forces. The fuzzy logic controller achieved reductions (over the LQG controller) in the required RMS control forces of about 25.66% and 22.64% over the wind direction angles 0° and 292.5°, respectively (at these directions the controllers required the highest control forces over all the wind direction angles). This indicates that the fuzzy logic controller may require smaller actuator compared to the LQG controller.

Table 4 lists the uncontrolled and controlled responses of the building in the y-direction under a wind attack angle of 0°. For security concerns, mean wind speed that corresponds to a return of 100 years is used. RMS and peak values of the displacement at the top corner of the building, RMS and peak values of the maximum inter-story drift, RMS and peak values of the shear loads (SL) at the ground level, and RMS and peak values of the bending moment (BM) at the ground level are considered. Percentages in the response reduction are indicated in the table (between brackets). Under wind loads with a return of 100 years, the TMD can achieve significant reductions in the displacements and the inter-story drift of the building. For security reasons, some designers require that the peak inter-story drift-ratio does not exceed 0.005 (Taranath 2005). However, the peak inter-story drift-ratio is shown to exceed the allowable design limit for the uncontrolled case. It is shown that both the TMD and the ATMD satisfied the security criteria. In addition, the design loads are significantly reduced with both devices. This indicates the capability of the TMD and the ATMD to protect high-rise buildings and to improve the structural resiliency under extreme wind loads.

Table 4 (a) Uncontrolled and controlled (with TMD) building responses for security reasons (y-direction at 0°, R = 100 years)

Criteria	Uncontrolled			TMD		
	+0%	+10%	-10%	+0%	+10%	-10%
RMS Disp. (m)	0.3499	0.3364	0.3571	0.1762 (49.64%)	0.1659 (50.68%)	0.1808 (49.37%)
Peak Disp. (m)	1.2295	1.0495	1.2649	0.6461 (47.45%)	0.7504 (28.50%)	0.6605 (47.78%)
Peak Drift (rad)	0.0066	0.0056	0.0068	0.0034 (48.48%)	0.0040 (28.57%)	0.0035 (48.53%)
RMS BS (N)	1.42E+7	1.24E+7	7.23E+6	7.46E+6 (46.34%)	6.68E+6 (47.48%)	5.50E+6 (46.05%)
Peak BS (N)	4.60E+7	4.22E+7	2.83E+7	3.19E+7 (41.79%)	2.60E+7 (30.68%)	2.49E+7 (38.42%)
RMS BM (N.m)	2.10E+9	1.83E+9	1.01E+9	1.04E+9 (49.47%)	9.28E+8 (50.36%)	7.24E+8 (49.17%)
Peak BM (N.m)	6.56E+9	6.45E+9	3.69E+9	4.65E+9 (46.26%)	3.34E+9 (29.15%)	3.26E+9 (48.25%)

Table 4 (b) Controlled (with ATMD) building responses for security reasons (y-direction at 0°, R = 100 years)

Criteria	ATMD with LQG			ATMD with Fuzzy		
	+0%	+10%	-10%	+0%	+10%	-10%
RMS Disp. (m)	0.1300 (62.85%)	0.1194 (64.51%)	0.1458 (59.1%)	0.1480 (57.7%)	0.1443 (57.10%)	0.1614 (54.80%)
Peak Disp. (m)	0.5871 (52.25%)	0.5752 (45.19%)	0.5998 (52.6%)	0.6664 (45.8%)	0.7598 (27.60%)	0.6191 (51.06%)
Peak Drift (rad)	0.0031 (53.03%)	0.0031 (44.64%)	0.0032 (52.9%)	0.0035 (47.0%)	0.0041 (26.79%)	0.0033 (51.47%)
RMS BS (N)	5.6E+6 (59.2%)	5.5E+6 (60.7%)	6.2E+6 (55.7%)	6.6E+6 (53.9%)	6.1E+6 (53.6%)	1.4E+7 (51.1%)
Peak BS (N)	2.6E+7 (48.7%)	2.5E+7 (44.6%)	2.7E+7 (41.9%)	3.2E+7 (44.0%)	2.5E+7 (30.9%)	4.6E+7 (40.5%)
RMS BM (N.m)	7.3E+8 (63.7%)	7.3E+8 (65.1%)	8.3E+8 (60.2%)	9.0E+8 (58.2%)	8.2E+8 (57.4%)	2.1E+9 (55.4%)
Peak BM (N.m)	3.5E+9 (52.5%)	3.0E+9 (46.2%)	3.8E+9 (53.3%)	4.7E+9 (44.7%)	3.2E+9 (28.2%)	6.6E+9 (50.7%)

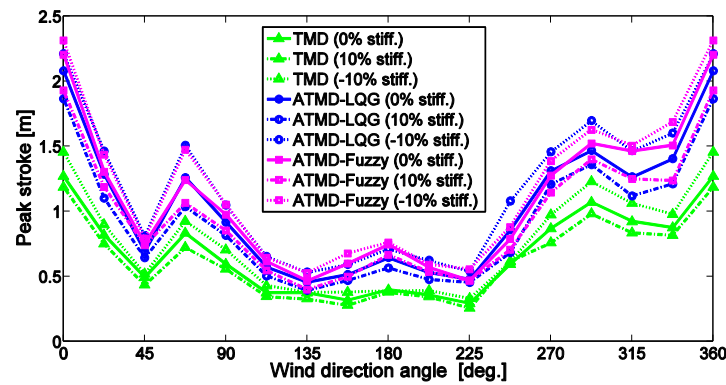


Fig. 20 Stroke (peak values) of the TMD in the y-direction

5.3 Comments

The current study has raised the following comments:

- The approach proposed in the current paper to choose the tuning parameters of the TMD is more generic. While the methods discussed in the literature allow for choosing optimal parameters for a specific optimization objective (displacement minimization), the proposed approach permits selecting the tuning parameters for different optimization objectives (e.g., minimizing acceleration and/or displacement) under different types of excitation inputs (wind or earthquake). In addition, the paper goes further into the direction of making the TMD more robust by introducing an active control force (forming the ATMD) with two controllers.

- Fig. 20 shows the stroke (peak values) of the ATMD for three cases: uncontrolled (passive TMD), controlled TMD with LQG controller (ATMD-LQG) and TMD controlled with a fuzzy logic controller (ATMD-Fuzzy). The figure shows that the stroke of the TMD is increased by adding an actuator (ATMD). The peak values of the strokes for both the LQG and the fuzzy logic controllers have similar trends over all the wind direction angles. However, the fuzzy logic controller showed slight increase in the stroke under the wind direction angle 0° .

- The building considered in the current study is symmetric in terms of mass and stiffness. In reality, the mass distribution over floors could be asymmetric due to workmanship, detailing of the structural components and/or non-structural components of buildings. However, such asymmetry is not known during the preliminary design stage of the building used in the current study. The response of the building under wind loads was assumed to be in the linear zone. Under the assumption of a linear behavior, the building stiffness may be considered uncoupled which permits studying the behavior in the lateral directions independently from torsion. Once the full-scale building is operational, on site decay measurements, along with modal analysis, may be used to properly model and analyze any significant (if any) coupled torsional translational response of the building under wind loads.

6. Conclusions

A robust passive and active TMD design was proposed for vibration reduction in high-rise buildings under wind loads. First, a numerical approach was followed to predetermine the optimum parameters of the TMD for a primary structure. Generic design charts were created for two optimization objectives (displacement and acceleration minimization) under two excitation inputs (wind and earthquake loads). Second, the optimum parameters were used to estimate the robust parameters for a structure with stiffness uncertainties. Finally, to show the capability of the proposed approach to improve the performance and the resiliency of high-rise buildings under multidirectional wind, a case study building was considered. Due to the slenderness of the building in one direction, active control of the TMD was a requisite (ATMD). LQG and fuzzy logic controllers were proposed for the ATMD. The main outcomes of the paper are summarized as follows:

- For the use of TMDs in high-rise buildings, optimal design parameters depend on the optimization objective as well as the input excitation (wind or earthquake). The response reduction in the primary structure and the robustness of the TMD increase with the increase of the mass ratio;
- Practical design parameters of the TMD can be different from the optimum ones. However,

predetermined optimal parameters for a primary structure with uncertainties are useful to attain design robustness. Comparisons between the controlled case (with TMD) and the uncontrolled case demonstrate the effectiveness of the proposed approach for buildings with frequency uncertainty, under multidirectional wind loads;

- The case study considered in the current paper presents an engineered design that is instructive. Due to unequal aspect ratios in the two lateral directions, the building required heavy mass for the TMD with actuators (ATMD) in one lateral direction, where it behaves like a cantilever structure, while two-thirds of the mass was sufficient in the other direction, where the behavior of the building is dominantly in shear. This leads to a conclusion that shear buildings may be controlled with less effort than cantilever buildings. Also, it can be concluded that structural control performance in high-rise buildings may depend on the shape of the building, hence the flow patterns, and the wind direction angle;

- For the use of the ATMDs, the performance of LQG and fuzzy logic controllers is remarkable in reducing the responses of high-rise buildings under multidirectional winds. However, the fuzzy logic controller is more robust than the LQG controller and may require a smaller actuator;

- In addition to reducing the top floor peak accelerations, for comfort reasons, the wind-induced loads are also reduced. This indicates the ability of the TMD and the ATMD to improve the performance and the resiliency of high-rise buildings under extreme wind loads.

References

- Aldawod, M., Samali, B., Naghdy, F. and Kwok K.C.S. (2001), "Active control of along wind response of tall building using a fuzzy controller", *Eng. Struct.*, **23**(11), 1512-1522.
- Aly, A.M. (2009), *On the dynamics of buildings under winds and earthquakes: response prediction and reduction*, Ph.D. Dissertation, Politecnico di Milano, Milan, Italy.
- Aly, A.M. and Christenson, R.E. (2008), "On the evaluation of the efficacy of a smart damper: a new equivalent energy-based probabilistic approach", *Smart Mater. Struct.*, **17**(4), Article ID: 045008.
- Aly, A.M., Zasso, A. and Resta, F. (2012), "Proposed configurations for the use of smart dampers with bracings in tall buildings", *Smart Mater. Res.*, Article ID: 251543. Doi:10.1155/2012/251543.
- Aly, A.M. (2012), "Proposed robust tuned mass damper for response mitigation in buildings exposed to multidirectional wind", *Struct. Des. Tall Spec.*, DOI: 10.1002/tal.1068.
- Aly, A.M., Zasso, A. and Resta, F. (2011a), "On the dynamics of a very slender building under winds: response reduction using MR dampers with lever mechanism", *Struct. Des. Tall Spec.*, **20**(5), 539-551. Doi: 10.1002/tal.647.
- Aly, A.M., Zasso, A. and Resta, F. (2011b), "Dynamics and control of high-rise buildings under multidirectional wind loads", *Smart Mater. Res.*, Article ID: 549621. Doi:10.1155/2011/549621.
- Aly, A.M., Resta, F. and Zasso, A. (2008), "Active control in a high-rise building under multidirectional wind loads", *Proceedings of the 2008 Structures Congress - Structures Congress 2008: Crossing the Borders*, American Society of Civil Engineers, Vancouver, BC, Canada, April 24-26. Doi: 10.1061/41016(314)285.
- Attaway, S. (2009), *Matlab: A practical introduction to programming and problem solving*, Butterworth-Heinemann, Amsterdam, Netherlands.
- Bani-Hani, K.A. (2007), "Vibration control of wind-induced response of tall buildings with an active tuned mass damper using neural networks", *Struct. Control. Health Monit.*, **14**(1), 83-108.
- Battaini, M., Casciati, F. and Faravelli, L. (1998), "Control algorithm and sensor location", *Proceedings of the 2nd World Conf. on Structural Control*, Kyoto, Japan, 28 June - 1 July.

- Bendat, J.S. and Piersol, A.G. (2000), *Random data analysis and measurement procedures*, 3rd Ed, Wiley Series in Probability and Statistics, New York, USA.
- Casciati, F. (1997), "Checking the stability of a fuzzy controller for nonlinear structures", *J. Microcomput. Civ. Eng.*, **12**(3), 205-215.
- Chowdhury, I. and Dasgupta, S. (2003), "Computation of Rayleigh damping coefficients for large systems", *The Electronic Journal of Geotechnical Engineering*, **8**, Bundle 8C.
- Clinton, J.F., Bradford, C.S., Heaton, T.H. and Favela, J. (2006), "The observed wander of the natural frequencies in a structure", *Bull Seismol. Soc. Amer.*, **96**(1), 237-57.
- Davison, E.J. (1966), "A method for simplifying linear dynamic systems", *IEEE T. Automat. Contr.*, **11**(1), 93-101.
- Dyke, S.J., Caicedo, J.M., Turan, G., Bergman, L.A. and Hague S. (2003), "Phase I benchmark control problem for seismic response of cable-stayed bridges", *J. Struct. Eng.*, **129**(7), 857-872.
- Eurocode 1. (2004), Eurocode 1: Actions on structures - General actions - Part 1-4: Wind actions. prEN 1991-1-4: European Standard.
- Feng, M.Q. and Mita, A. (1995), "Vibration control of tall buildings using mega subconfiguration", *J. Eng. Mech. - ASCE*, **121**(10), 1082-1088.
- Ghorbani-Tanha, A.K., Noorzad, A. and Rahimian, M. (2009), "Mitigation of wind-induced motion of Milad tower by tuned mass damper", *Struct. Des. Tall Spec.*, **18**, 371-385. Doi: 10.1002/tal.421.
- Gu, M. and Peng, F.J. (2002), "An experimental study of active control of wind-induced vibration of super-tall buildings", *J. Wind Eng. Ind. Aerod.*, **90**(12-15), 1919-1931.
- Lee, J.J., and Yun, C.B. (2006), "Damage diagnosis of steel girder bridges using ambient vibration data", *Eng. Struct.*, **28**(6), 912-925.
- Li, C., Li, J. and Qu, J. (2010), "An optimum design methodology of active tuned mass damper for asymmetric structures", *Mech. Syst. Signal Pr.*, **24**(3), 746-765.
- Li, C. and Zhu, B. (2006), "Estimating double tuned mass dampers for structures underground acceleration using a novel optimum criterion", *J. Sound Vib.*, **298**(1-2), 280-297.
- Li, Q.S., Yang, K., Zhang, N., Wong, C.K. and Jeary, A.P. (2002), "Field measurement of amplitude dependent damping in a 79-storey tall building and its effects on the structural dynamic responses", *Struct. Des. Tall Spec.*, **11**, 129-153.
- Liu, C. and DeWolf, J.T. (2007), "Effect of temperature on modal variability of a curved concrete bridge under ambient loads", *J. Struct. Eng.*, **133**(12), 1742-1751.
- Lu, L., Chiang, W., Tang, J., Liu, M. and Chen, C. (2003), "Active control for a benchmark building under wind excitations", *J. Wind Eng. Ind. Aerod.*, **91**(4), 469-493. Doi: 10.1016/S0167-6105(02)00431-2.
- Lu, X., Li, P., Guo, X., Shi, W. and Liu, J. (2012), "Vibration control using ATMD and site measurements on the Shanghai World Financial Center Tower", *Struct. Des. Tall Spec.*, Doi: 10.1002/tal.1027.
- Marazzi, F. and Magonette, G. (2001), *Active and semi-active control of structures: a comparison*, European Meeting on Intelligent Structures, Ischia, Italy.
- Meirovitch, L. (1967), *Analytical methods in vibrations*, The Macmillan Co., New York.
- Metwally, H.M., El-Souhily, B.M. and Aly, A. (2006), "Reducing vibration effects on buildings due to earthquake using magneto-rheological dampers", *Alex. Eng. J.*, **45**(2), 131-140.
- Rosa, L., Tomasini, G., Zasso, A. and Aly, A.M. (2012), "Wind-induced dynamics and loads in a prismatic slender building: a modal approach based on unsteady pressure measurements", *J. Wind Eng. Ind. Aerod.*, **107-108**, 118-130.
- Satake, N., Suda, K., Arakawa, T., Sasaki, A. and Tamura, Y. (2003), "Damping evaluation using full-scale data of building in Japan", *J. Struct. Eng. - ASCE*, **129**(4), 470-477.
- Samali, B., Al-Dawod, M., Kwok K.C. and Naghdy, F. (2004), "Active control of cross wind response of 76-story tall building using a fuzzy controller", *J. Eng. Mech. - ASCE*, **130**(4), 492-498.
- Skelton, R. E. (1988). *Dynamic systems control: Linear systems analysis and synthesis*, Wiley, New York.
- Smith R.J. and Willford, M.R. (2007), "The damped outrigger concept for tall buildings", *Struct. Des. Tall Spec.*, **16**(4), 501-517.
- Sohn, H., Dzwonczyk, M., Straser, E.G., Kiremidjian, A.S., Law K.H. and Meng, T. (1999), "An

- experimental study of temperature effect on modal parameters of the Alamosa Canyon Bridge”, *Earthq. Eng. Struct. D.*, **28**(8), 879-97.
- Spencer, B.F., Jr., Dyke, S.J. and Deoskar, H.S. (1998), “Benchmark problems in structural control. I: Active mass driver system, and II: Active tendon system”, *Earthq. Eng. Struct. D.*, **27**(11), 1127-1147.
- Tamura, Y. and Yoshida, A. (2008), “Amplitude dependency of damping in buildings”, *Proceedings of the 18th Analysis and Computation Specialty Conference*, Vancouver, Canada.
- Taranath, B.S. (2005), *Wind and earthquake resistant buildings: structural analysis and design*, Marcel Dekker, New York.
- Warburton, G.B. and Ayorinde, E.O. (1980), “Optimum absorber parameters for simple systems”, *Earthq. Eng. Struct. D.*, **8**(3), 197-217.
- Wu, J.C., Yang, J.N., Schmitendorf, W. (1998), “Reduced-order H_∞ and LQR control for wind-excited tall buildings”, *Eng. Struct.*, **20**(3), 222-236.
- Xia, Y., Hao, H., Zanardo, G. and Deeks, A., (2006), “Long term vibration monitoring of an RC slab: temperature and humidity effect”, *Eng. Struct.*, **28**(3), 441-52.
- Yan, J., Ryan, M., and Power, J. (1994), *Using Fuzzy Logic: Towards Intelligent Systems*, Prentice Hall, New York.
- Yang, J.N., Agrawal, A.K., Samali, B. and Wu, J.C. (2004), “Benchmark problem for response control of wind-excited tall buildings”, *J. Eng. Mech.- ASCE*, **130**(4), 437-446.
- Yuen, K.V. and Kuok, S.C. (2010a), “Ambient interference in long-term monitoring of buildings”, *Eng. Struct.*, **32**(8), 2379-2386.
- Yuen, K.V. and Kuok, S.C. (2010b), “Modeling of environmental influence in structural health assessment for reinforced concrete buildings”, *Earthq. Eng. Eng. Vib.*, **9**(2), 295-306.
- Zasso, A., Aly, A.M., Rosa, L. and Tomasini, G. (2008), “Wind induced dynamics of a prismatic slender building with 1:3 rectangular section”, *Proceedings of the BBAA VI International Colloquium on Bluff Bodies Aerodynamics & Applications*, Milano, Italy, 20-24 July.